

Pulse shaping of bright-dark vector soliton pair

Yan Zhou(周延), Yuefeng Li(李月锋), Xia Li(李夏), Meisong Liao(廖梅松), Jingshan Hou(侯京山), Yongzheng Fang(房永征)

Citation: Chin. Phys. B . 2020, 29(5): 054202 . **doi:** 10.1088/1674-1056/ab7b56
Journal homepage: http://cpb.iphy.ac.cn; http://iopscience.iop.org/cpb

What follows is a list of articles you may be interested in

Effect of thermally induced birefringence on high power picosecond azimuthal polarization Nd:YAG laser system

Hongpan Peng(彭红攀), Ce Yang(杨策), Shang Lu(卢尚), Ning Ma(马宁), Meng Chen(陈檬)
Chin. Phys. B . 2019, 28(2): 024205 . **doi:** 10.1088/1674-1056/28/2/024205

Polarization-based range-gated imaging in birefringent medium:Effect of size parameter

Heng Tian(田恒), Jing-Ping Zhu(朱京平), Shu-Wen Tan(谭树文), Jing-Jing Tian(田晶晶), Yun-Yao Zhang(张云尧), Xun Hou(侯洵)
Chin. Phys. B . 2018, 27(12): 124203 . **doi:** 10.1088/1674-1056/27/12/124203

Birefringence via Doppler broadening and prevention of information hacking

Humayun Khan, Muhammad Haneef, Bakhtawar
Chin. Phys. B . 2018, 27(1): 014201 . **doi:** 10.1088/1674-1056/27/1/014201

Design of photonic crystal fiber with elliptical air-holes to achieve simultaneous high birefringence and nonlinearity

Min Liu(刘敏), Jingyun Hou(侯静云), Xu Yang(杨虚), Bingyue Zhao(赵昺玥), Ping Shum
Chin. Phys. B . 2018, 27(1): 014206 . **doi:** 10.1088/1674-1056/27/1/014206

Electro-optical properties of high birefringence liquid crystal compounds with isothiocyanate and naphthyl group

Zeng-Hui Peng(彭增辉), Qi-Dong Wang(王启东), Shao-Xin Wang(王少鑫), Li-Shuang Yao(姚丽双), Yong-Gang Liu(刘永刚), Li-Fa Hu(胡立发), Zhao-Liang Cao(曹召良), Quan-Quan Mu(穆全全), Cheng-Liang Yang(杨程亮), Li Xuan(宣丽)
Chin. Phys. B . 2017, 26(9): 094210 . **doi:** 10.1088/1674-1056/26/9/094210

Pulse shaping of bright–dark vector soliton pair*

Yan Zhou(周延)[1,†], Yuefeng Li(李月锋)[1], Xia Li(李夏)[2], Meisong Liao(廖梅松)[2], Jingshan Hou(侯京山)[3], and Yongzheng Fang(房永征)[3]

[1] School of Science, Shanghai Institute of Technology, Shanghai 201418, China
[2] Key Laboratory of Materials for High Power Laser, Shanghai Institute of Optics and Fine Mechanics, Chinese Academy of Sciences, Shanghai 201800, China
[3] School of Materials Science and Engineering, Shanghai Institute of Technology, Shanghai 201418, China

(Received 5 January 2020; revised manuscript received 19 January 2020; accepted manuscript online 1 March 2020)

We simulate pulse shaping of bright–dark vector soliton pair in an optical fiber system. Through changing input pulse parameters (amplitude ratio, projection angle, time delay, and phase difference), different kinds of pulse shapes and spectra can be generated. For input bright–dark vector soliton pair with the same central wavelength, "2 + 1"- and "2 + 2"-type pseudo-high-order bright–dark vector soliton pairs are achieved. While for the case of different central wavelengths, bright–dark vector soliton pairs with multiple pulse peaks/dips are demonstrated with appropriate pulse parameter setting.

Keywords: bright–dark vector soliton, birefringence, polarization-locking, group-velocity-locking

PACS: 42.25.Ja, 42.25.Lc, 42.55.Wd, 42.65.–k **DOI:** 10.1088/1674-1056/ab7b56

1. Introduction

Optical soliton is a kind of localized nonlinear wave in nonlinear optical systems, and it can propagate along long distances without pulse shape distortion. Optical solitons have been widely studied theoretically and experimentally. In theory, soliton solutions can be obtained by solving nonlinear Schrödinger equation (NLSE) and Ginzburg–Landau equation (GLE).[1] When the amplitude modulations (including gain, loss, spectral filtering, and saturable absorption) in GLE are negligible, GLE can be approximated with NLSE. While in experiments, optical solitons can be achieved in passively mode-locked solid-state and fiber lasers. Especially, solitons in ultrafast fiber laser field have been attracting much attention, because of the unique characteristics (including dispersion, nonlinearity, gain, and loss) offered by single-mode and multi-mode fibers. Currently, many researches are focused on optical solitons in single-mode fiber lasers, because of their compactness, stability, ease of maintenance, and so on. Until now, different kinds of optical solitons that exist in fiber lasers have been theoretically solved and experimentally demonstrated, such as traditional soliton,[2,3] dispersion-managed soliton,[4,5] self-similariton,[6,7] dissipative solion,[8,9] dual-wavelength domain wall soliton,[10] and so on.[11–14] They can be generated by appropriate design of intra-cavity parameters. Also, multi-state solitons can be emitted in bidirectional mode-locked fiber lasers.[15] As the development of detection techniques, soliton dynamics can be explored with time-stretch dispersive Fourier transform (TS-DFT) technique,[16–19] which reveals the transient dynamics of soliton evolution and building processes.

In reality, single-mode-fiber is anisotropic even with circular symmetry, because of material imperfections and external environmental disturbance (such as stress and heat flow). So scalar approximation is not applicable and coupled NLSEs and GLEs should be considered for solving.[20] In this situation, various vector solitons could be generated, such as polarization/phase-locked vector soliton (PLVS),[21–23] group-velocity-locked vector soliton (GVLVS),[24–27] polarization rotation vector soliton (PRVS),[28,29] and so on, depending on the strength of intra-cavity linear birefringence and cross-phase modulation (XPM). Also, we can classify the vector solitons according to their pulse waveforms, such as bright–bright vector soliton, bright–dark vector soliton and dark–dark vector soliton. Bright soliton has a temporal intensity peak, while dark soliton has a temporal intensity dip with continuous light background. Vector solitons have potential applications in optical communications and optical data processing.[30,31]

In previous works, many different kinds of vector solitons have already been observed in mode-locked fiber lasers. For example, coherently and incoherently coupled bright–dark vector solitons in single-mode fiber lasers were experimentally shown.[32,33] Simulation about generating pseudo-high-order polarization-locked vector soliton was reported.[34] Manipulation of polarization- and group-velocity-locked dark vector solions was also theoretically simulated.[35] However, there are few reports about the pulse shaping of bright–dark vector soliton pair. In this paper, we simulate the pulse shaping of bright–dark vector solion pair in a polarization insensitive optical fiber system. Through changing input pulse parameters, different kinds of pulse shapes and optical spectra in or-

*Project supported by the National Key Research and Development Program of China (Grant No. 2018YFB0504500) and the National Natural Science Foundation of China (Grant No. 51672177).

†Corresponding author. E-mail: yzhou@sit.edu.cn

© 2020 Chinese Physical Society and IOP Publishing Ltd

thogonal polarization directions can be generated. Our simulation result further explore the vector properties of optical soliton, and can provide beneficial conduct for latter experiments about pulse shaping of bright–dark vector soliton pair at different wavelengths.

2. Simulation

Figure 1 is the depiction of our theoretical model. It is a polarization-insensitive optical fiber system. "A_2/A_1 change" section is used for changing amplitude ratio of orthogonal modes and it can be adjusted by fiber amplifier or fiber attenuator; "ΔT change" section is for changing time delay between orthogonal modes and it can be changed with optical fiber time delay line; SMF is single-mode-fiber; PC (polarization controller) is for changing linear fiber birefringence; Col (collimator) is employed for collimating laser beam; PBS (polarization beam splitter) can separate orthogonally polarized electric fields and can also be rotated to change projection angle between the polarization direction and the projection axes. Bright–dark vector soliton pair passes through different stages one by one in order, and finally detected by photo-detector after passing through or being reflected by the PBS. $A_{\text{horizontal}}$ and A_{vertical} stand for the amplitude projection along horizontal and vertical polarization directions.

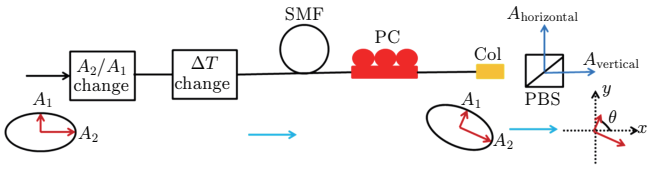


Fig. 1. Picture of theoretical model.

Firstly, the temporal pulse amplitudes $A_1(t)$ and $A_2(t)$ of incident bright–dark vector solion pair in orthogonal polarization directions can be expressed as

$$A_1(t) = A_1 \operatorname{sech}\left[\frac{1.763(t-\Delta T/2)}{T_1}\right] \times \exp\left(\mathrm{i}\frac{2\pi ct}{\lambda_1}\right), \tag{1}$$

$$A_2(t) = A_2 \tanh\left[\frac{1.763(t+\Delta T/2)}{T_2}\right] \times \exp\left(\mathrm{i}\left(\frac{2\pi ct}{\lambda_2}+\Delta\varphi\right)\right). \tag{2}$$

In Eqs. (1) and (2), we make the assumption that horizontal mode is black soliton with "tanh"-type pulse shape, and vertical mode is bright soliton with "sech"-type pulse shape. A_1 and A_2 are amplitudes in vertical and horizontal polarization directions; t is time parameter; ΔT stands for time delay between orthogonal modes; T_1 and T_2 are pulse widths for vertical and horizontal mode; c is light velocity in a vacuum; $\Delta\varphi$ is phase difference between orthogonal modes and it includes two parts: one is the phase difference of incident orthogonal polarization modes, the other is the linear birefringence-induced phase difference imposed in the optical fiber system; λ_1 and λ_2 are central wavelengths of orthogonal modes. We assume the projection angle is θ, then the projected amplitudes along horizontal and vertical polarization directions can be calculated according to

$$A_{\text{horizontal}} = A_1(t)\cos\theta + A_2(t)\sin\theta, \tag{3}$$

$$A_{\text{vertical}} = A_1(t)\sin\theta - A_2(t)\cos\theta. \tag{4}$$

In the latter simulation, we let $T_1 = T_2 = 5$ ps and simulate the temporal pulse shapes and optical spectra of output horizontal and vertical polarization modes, through changing amplitude ratio, projection angle, time delay and phase difference for orthogonal modes. The simulation results include two parts: the first is considering orthogonal modes with the same central wavelength, and the second one considers those with different central wavelengths.

2.1. $\lambda_1 = \lambda_2 = 1064$ nm

In this section, we assume $\lambda_1 = \lambda_2 = 1064$ nm. The 1064-nm central wavelength is selected because it can be generated in Yb-doped mode-locked fiber laser experimentally. Firstly, we consider the case when input amplitude ratio of bright–dark soliton pair is changed, and the corresponding simulation result is shown in Fig. 2. Here, we simulate the changes of output pulse shapes and optical spectra when amplitude ratio (A_2/A_1) is decreased from 3/1 to 1/3. Other variables are set as: $\theta = 0°$, $\Delta T = 0$ ps, and $\Delta\varphi = \pi/2$. The phase difference is fixed at $\pi/2$, which is the typical characteristic of PLVS with $\pm\pi/2$ phase difference in ytterbium fiber laser. The output pulse shapes in orthogonal polarization directions (see Figs. 2(a)–2(e)) shows the same tendency with amplitude ratio. While for optical spectra in Figs. 2(f)–2(j), both horizontal and vertical polarization modes have the same 3-dB bandwidth with different peak intensities. And the peak intensity is still different even though with the same input amplitude for orthogonal polarization modes. In all the simulated optical spectra, the optical spectrum resolution is ~ 0.15 nm.

Then, we consider the change of projection angle θ. Other variables are: $A_1 = A_2 = 1$, $\Delta T = 3$ ps, and $\Delta\varphi = \pi/2$. In Figs. 3(a)–3(e), we can see that as θ increases from 15° to 70°, the peak/dip pulse shape in horizontal/vertical direction will gradually evolve into dip/peak pulse shape. Besides, "2+2"-type pseudo-high-order bright–dark vector soliton pair occurs when $\theta = 44.5°$. We call it "pseudo-high-order" rather than "high-order" because the phase of amplitude projection along two principle axes of PBS is not locked. It should be noted that the pulse shapes in orthogonal polarization directions will coincide with each other when $\theta = 45°$ because of

symmetry projection. Besides, there is only one peak or dip in one polarization direction when $\Delta T = 0$ ps. The peak/dip of bright/dark soliton is not equal to one/zero because of energy transfer between horizontal mode and vertical mode. For output optical spectra in Figs. 3(f)–3(j), both orthogonal polarization modes have different 3-dB bandwidth and slight peak intensity difference. Horizontal mode has narrower/broader bandwidth when θ is smaller/larger than 45°, but the critical point is different for optical spectrum peak intensity.

After that, we simulate the pulse shapes and optical spectra when time delay ΔT is changed from 1 ps to 10 ps. Others are: $A_1 = A_2 = 1$, $\theta = 10°$, and $\Delta\varphi = \pi/2$. The corresponding simulation results are demonstrated in Figs. 4 and 5. In Fig. 4, the time separation of bright and dark solitons increases because the increasing ΔT value. Besides, the dark soliton in vertical polarization is gray soliton or black soliton, depending on ΔT. For optical spectra in Fig. 5, the peak intensity of orthogonal polarization modes is almost unchanged, accompanied with intensity difference ~ 3 dB. The centering wavelength is 1064 nm and 3-dB bandwidth is smaller than 1 nm for both polarization modes, but the bandwidth is larger compared with Fig. 3.

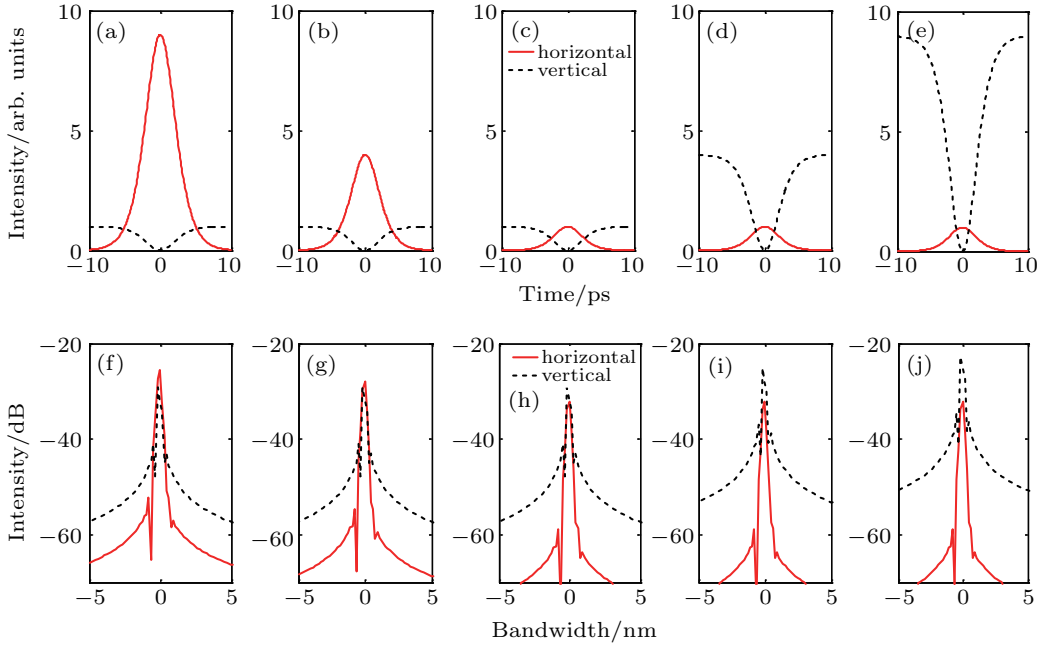


Fig. 2. Simulated output pulse shapes [(a)–(e)] and optical spectra [(f)–(j)] in orthogonal polarization directions when input amplitude ratio (A_2/A_1) is set as: 3/1, 2/1, 1/1, 1/2, and 1/3. Others are: $\theta = 0°$, $\Delta T = 0$ ps, and $\Delta\varphi = \pi/2$.

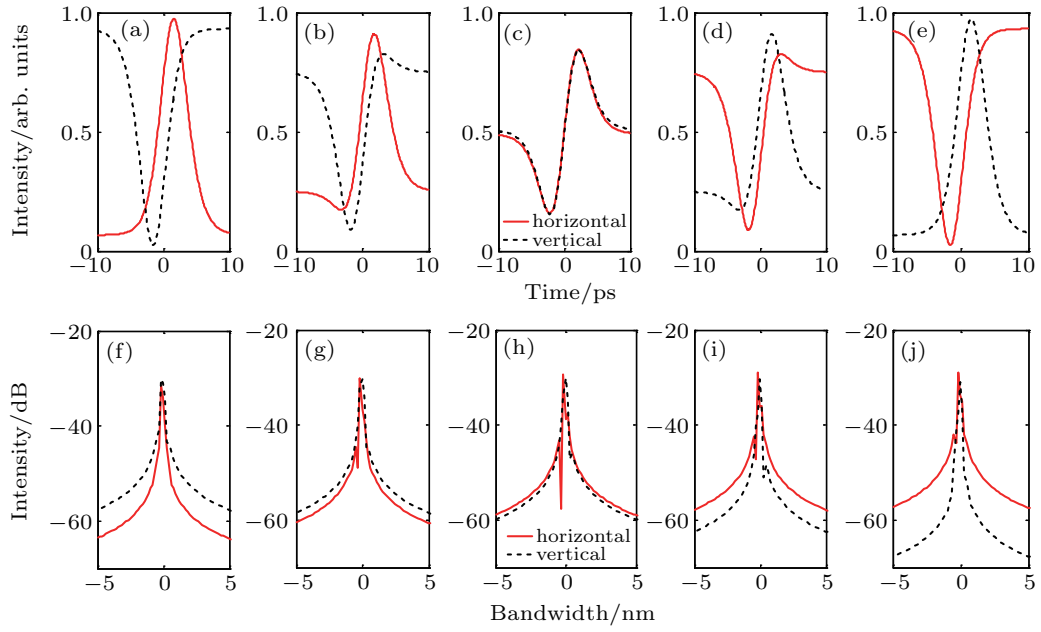


Fig. 3. Simulated output pulse shapes [(a)–(e)] and optical spectra [(f)–(j)] in orthogonal polarization directions when projection angle θ is set as: 15°, 30°, 44.5°, 60°, and 75°. Others are: $A_1 = A_2 = 1$, $\Delta T = 3$ ps, and $\Delta\varphi = \pi/2$.

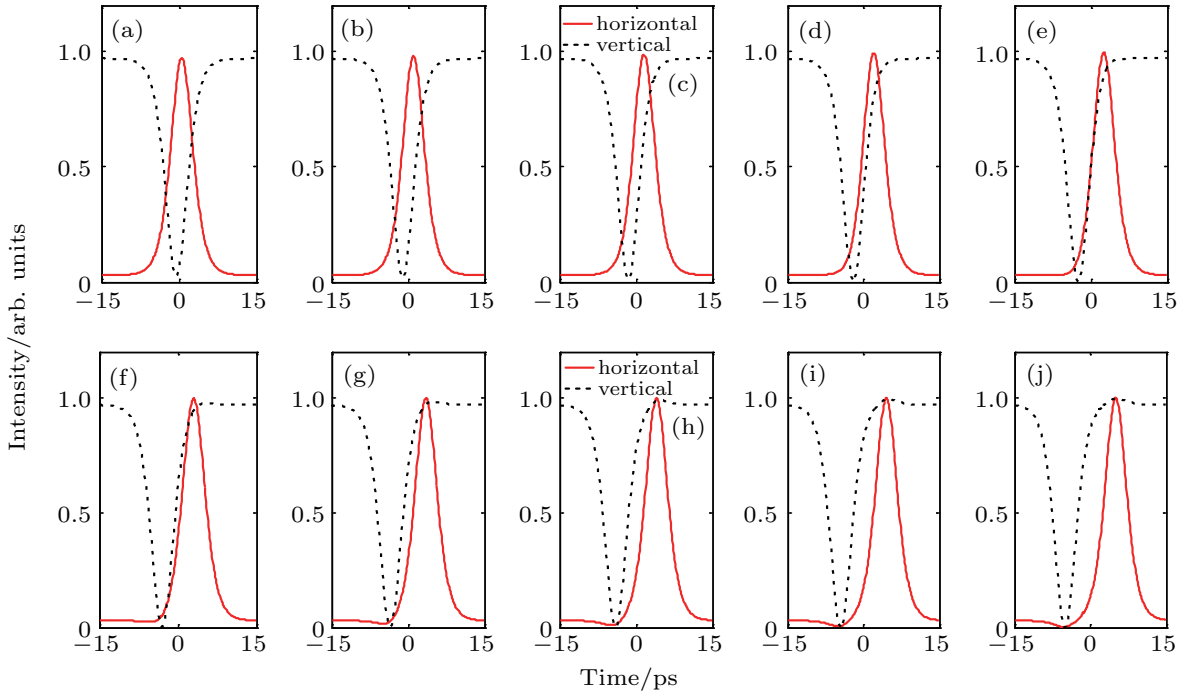


Fig. 4. Simulated output pulse shapes [(a)–(j)] in orthogonal polarization directions when time delay ΔT increases from 1 ps to 10 ps (1-ps time interval). Others are: $A_1 = A_2 = 1$, $\theta = 10°$, and $\Delta\varphi = \pi/2$.

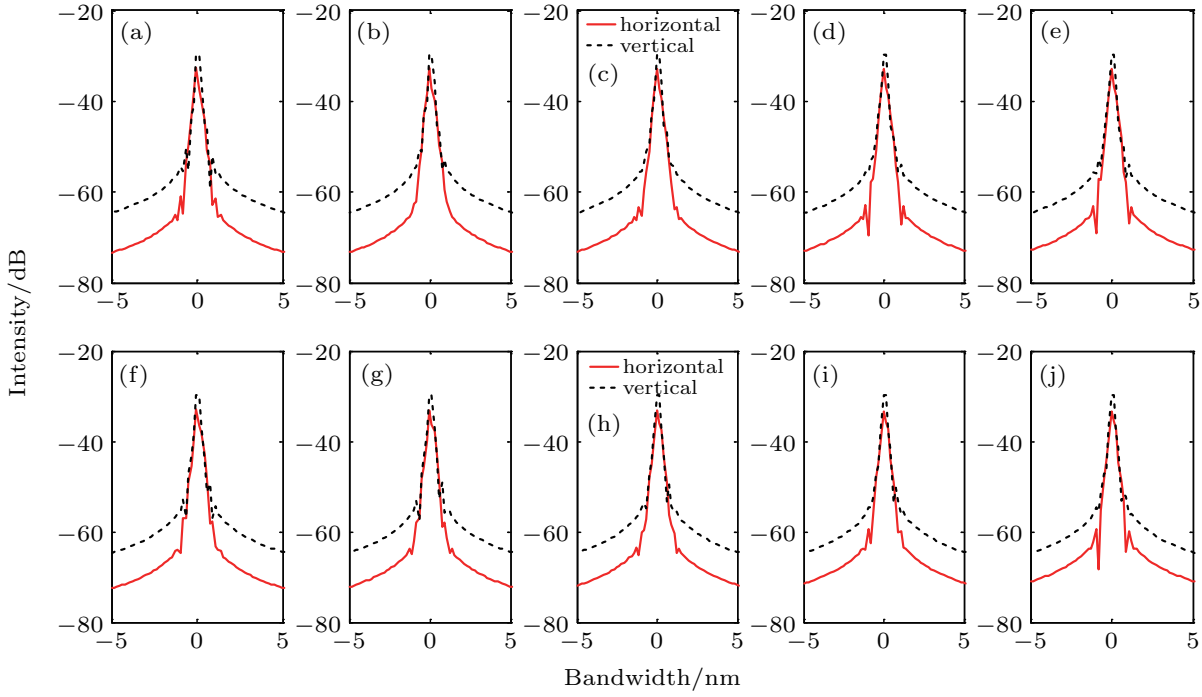


Fig. 5. Simulated output optical spectra [(a)–(j)] in orthogonal polarization directions when time delay ΔT increases from 1 ps to 10 ps (1-ps time interval). Others are the same as those in Fig. 4.

At last, we consider the influence of the phase difference $\Delta\varphi$ on the output pulse properties. Figure 6 shows the simulation result when $\Delta\varphi$ is increased from 0 to π. From pulse shapes of Figs. 6(a)–6(e), we can see that the peak intensity of horizontal bright soliton decreases with the increased $\Delta\varphi$. While for the vertical dark soliton, the dip intensity is almost unchanged, and another peak appears when $\Delta\varphi$ reaches to $3\pi/4$, which means that the "$1+2$"-type pseudo-high-order bright–dark vector soliton pair can be generated with appropriate $\Delta\varphi$ value. Besides, the vertical dark soliton is always black soliton with all $\Delta\varphi$ values. Figures 6(f)–6(j) are the corresponding optical spectra, and the figures show that the peak intensities of horizontal/vertical polarization modes have slight increase with the increased $\Delta\varphi$, and meanwhile, the peak intensity differences increase from 1.6 dB to 4.0 dB.

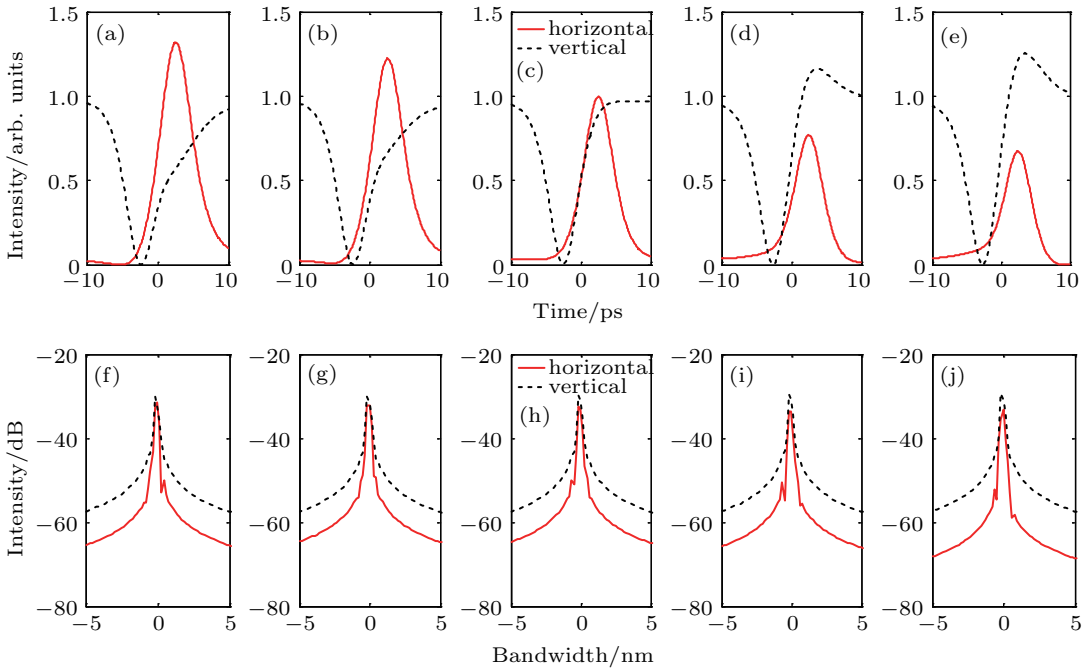


Fig. 6. Simulated output pulse shapes [(a)–(e)] and optical spectra [(f)–(j)] in orthogonal polarization directions when $\Delta\varphi$ is set as 0, $\pi/4$, $\pi/2$, $3\pi/4$, and π. Others are: $A_1 = A_2 = 1$, $\theta = 10°$, and $\Delta T = 5$ ps.

2.2. $\lambda_1 = 1063$ nm, $\lambda_2 = 1065$ nm

In this section, we simulate the output pulse shapes and optical spectra when $\lambda_1 \neq \lambda_2$, which is the characteristic of GVLVS. Because for GVLVS, the two orthogonal polarization modes will shift their central wavelengths, combining with self-phase modulation (SPM) and XPM to compensate linear intra-cavity fiber birefringence. In later simulations, we set $\lambda_1 = 1063$ nm and $\lambda_2 = 1065$ nm, and the simulation procedure is similar to the former case when $\lambda_1 = \lambda_2$. Firstly, the amplitude ratio (A_2/A_1) of incident pulses is decreased from 3/1 to 1/3, and others are set as: $\theta = 0°$, $\Delta T = 0$ ps, and $\Delta\varphi = 0$. The simulation result is shown in Fig. 7. We can see that both pulse shape and optical spectrum amplitudes of orthogonal polarization modes have the same tendency with A_2/A_1 change. For output optical spectra, the horizontal mode with red color always has only one peak, while vertical mode always has two peaks, which is different from the case when $\lambda_1 = \lambda_2$.

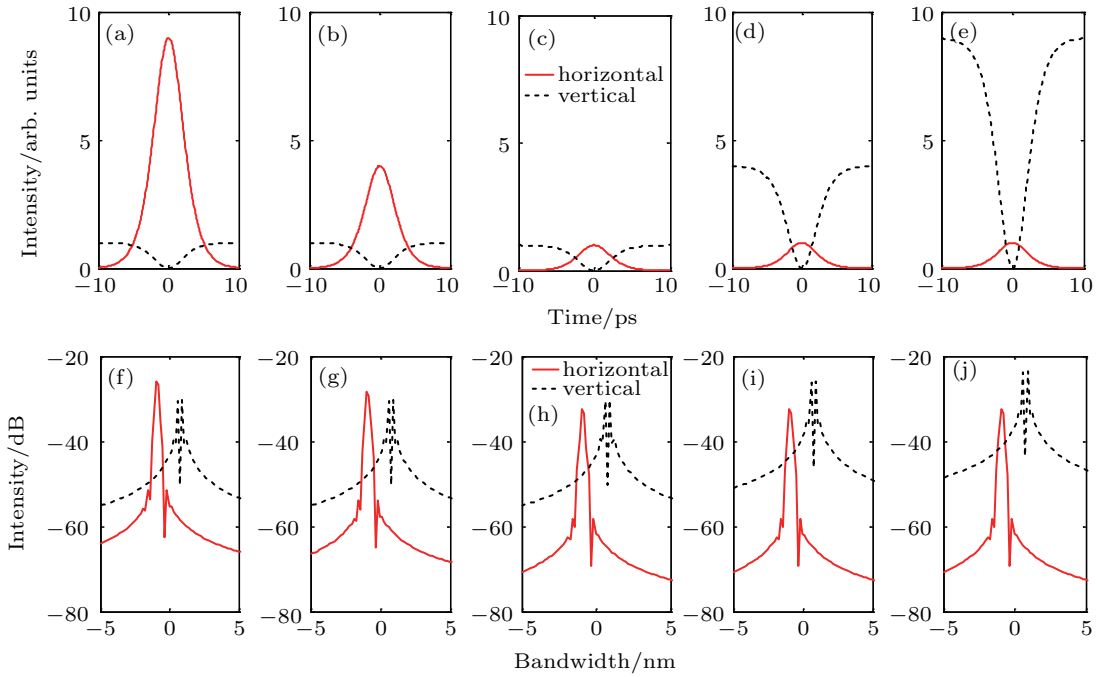


Fig. 7. Simulated output pulse shapes [(a)–(e)] and optical spectra [(f)–(j)] in orthogonal polarization directions when amplitude ratio (A_2/A_1) is set as: 3/1, 2/1, 1/1, 1/2, and 1/3. Others are: $\theta = 0°$, $\Delta T = 0$ ps, and $\Delta\varphi = 0$.

Then, we change projection angle θ and simulate the pulse shaping properties for incident group-velocity-locked bright–dark vector soliton pair. Figure 8 shows the corresponding simulation result when θ is increased from 15° to 75°, and other parameters are fixed at: $A_1 = A_2 = 1$, $\Delta T = 0$ ps, and $\Delta\varphi = 0$. In Figs. 8(a)–8(e), it shows that both orthogonal modes have only one peak/dip with multiple side pulse oscillations when $\theta = 15°$. When $\theta = 40°$, side pulse oscillations become obvious and the main peak/dip is undistinguishable, chirp-like pulses appear in horizontal and vertical polarization directions. And the orthogonal polarization modes will have the same temporal oscilloscope and the pedestal value is equal to 0.5 when $\theta = 45°$. For output optical spectra in Figs. 8(f)–8(j), both orthogonal modes have two peaks orientated at 1063 nm and 1067 nm. The red-shift of 1065 nm to 1067 nm may attribute to the energy transfer through amplitude projection along the two PBS axes. When θ is smaller than 45°, the horizontal mode has higher/lower peak intensity at 1063 nm/1067 nm wavelength position compared with vertical mode, and the result will become contrary when θ is larger than 45°. The orthogonal polarization modes have the same peak intensity at the above-mentioned two wavelengths when $\theta = 45°$ because of the projection symmetry.

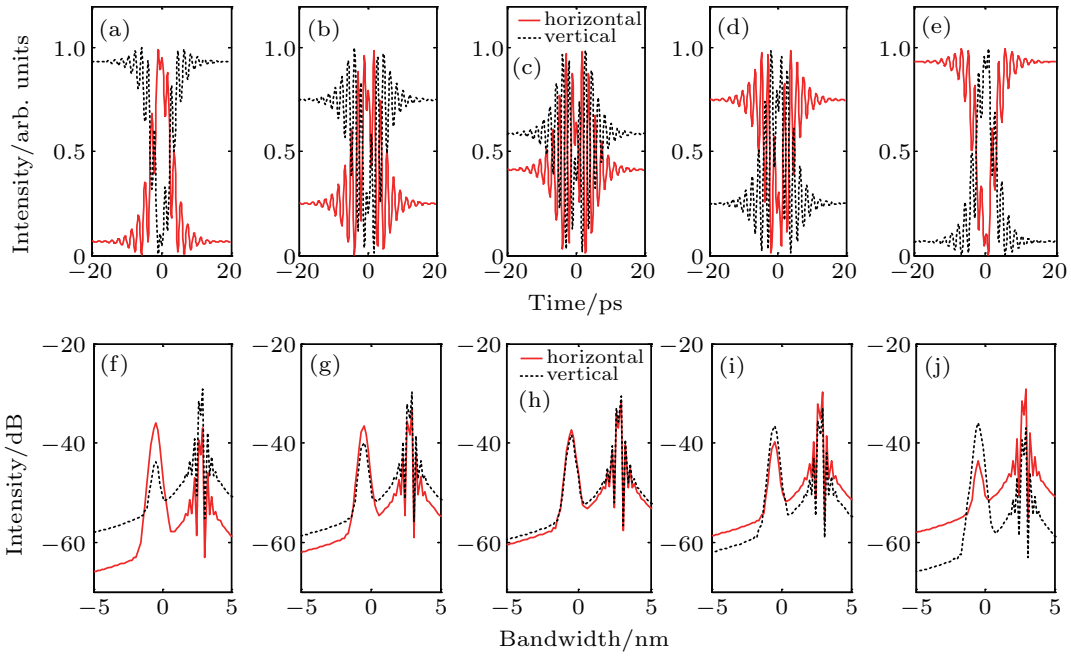


Fig. 8. Simulated output pulse shapes [(a)–(e)] and optical spectra [(f)–(j)] in orthogonal polarization directions when projection angle θ is set as: 15°, 30°, 40°, 60°, and 75°. Others are: $A_1 = A_2 = 1$, $\Delta T = 0$ ps, and $\Delta\varphi = 0$.

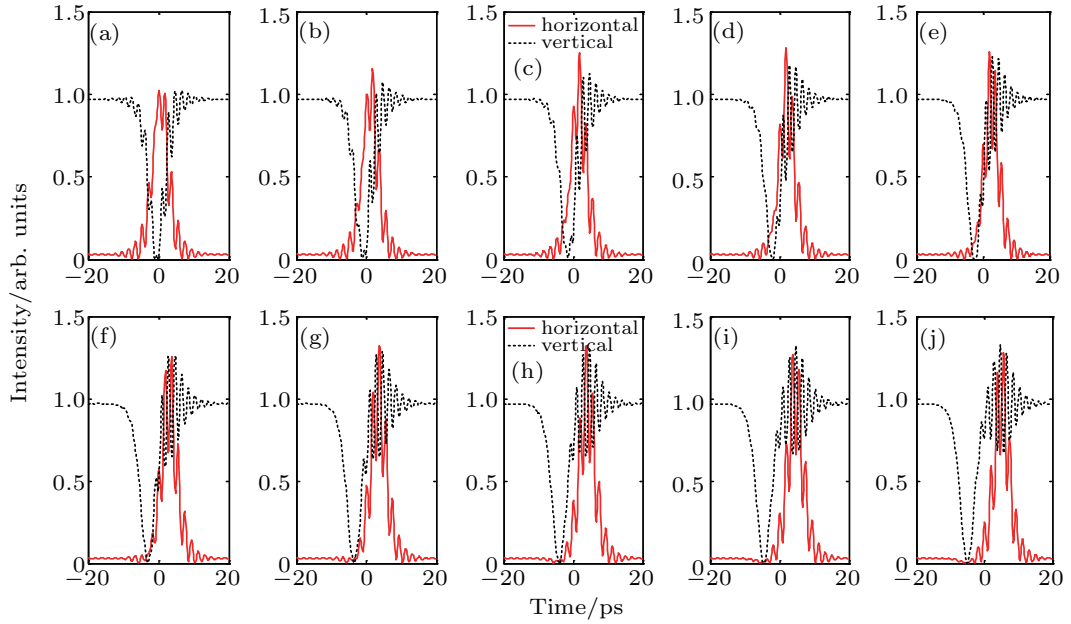


Fig. 9. Simulated output pulse shapes [(a)–(j)] in orthogonal polarization directions when time delay ΔT increases from 1 ps to 10 ps (1-ps time interval). Others are: $A_1 = A_2 = 1$, $\theta = 10°$, and $\Delta\varphi = 0$.

After that, the time delay ΔT is changed while with other variables fixed at appropriate values. ΔT increases from 1 ps to 10 ps while others are set as: $A_1 = A_2 = 1$, $\theta = 10°$, and $\Delta\varphi = 0$. The simulation results are demonstrated in Fig. 9 and Fig. 10. In Fig. 9, we can see the horizontal mode is always bright soliton pulse with multiple side peaks across the whole temporal pulse shape. The peak intensity increases when ΔT is increased from 1 ps to 4 ps, and will have slight oscillation in latter 6 ps. For vertical mode, the dark soliton pulse is always black soliton, and as the increase of the time delay, chirp-like oscillated multiple-pulses appear at the pulse trailing edge and they become obvious when ΔT is larger than 2 ps. Figure 10 is the corresponding simulated output optical spectra. It shows that both orthogonal modes have two wavelength bands at 1063 nm and red-shifted 1067 nm, which is similar to the case with angle changes. Besides, the peak intensity of the horizontal mode is always higher/lower than the vertical mode at 1063 nm/1067 nm with different time delay values.

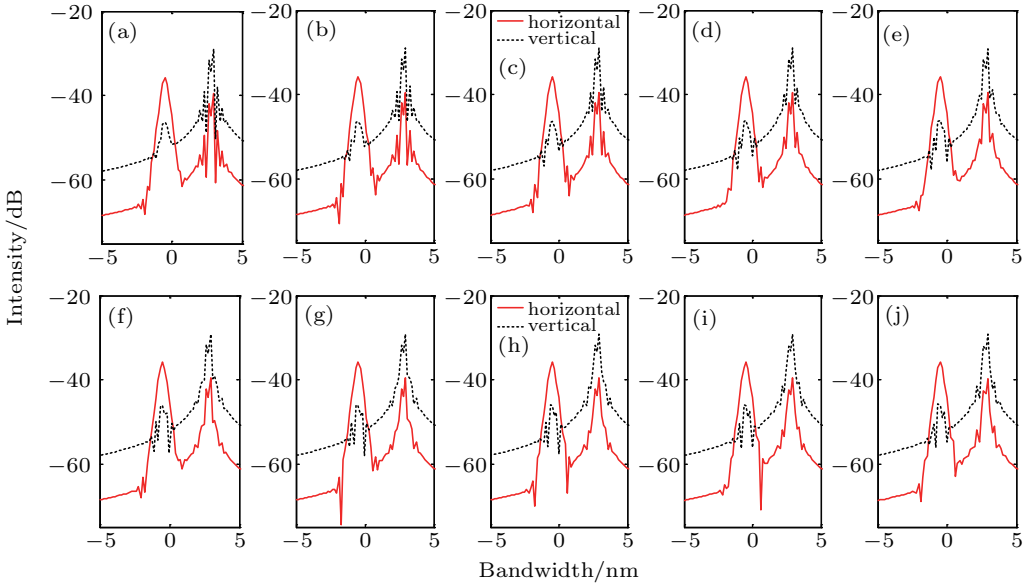


Fig. 10. Simulated output optical spectra [(a)–(j)] in orthogonal polarization directions when time delay ΔT increases from 1 ps to 10 ps (1-ps time interval). Others are the same as those in Fig. 9.

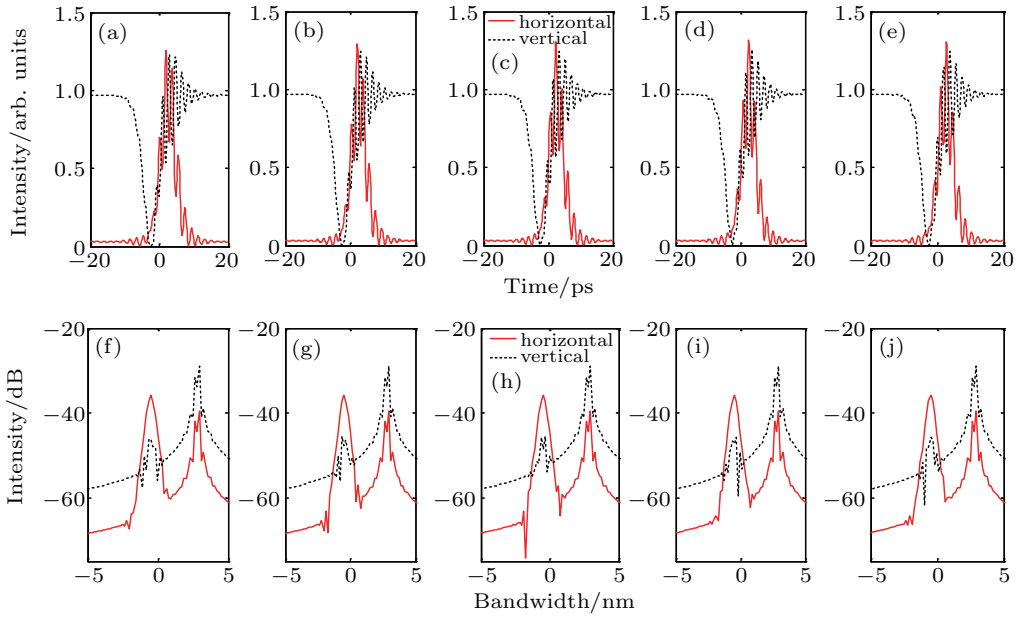


Fig. 11. Simulated output pulse shapes [(a)–(e)] and optical spectra [(f)–(j)] in orthogonal polarization directions when $\Delta\varphi$ is set as 0, $\pi/4$, $\pi/2$, $3\pi/4$, and π. Others are: $A_1 = A_2 = 1$, $\theta = 10°$, and $\Delta T = 5$ ps.

At last, we simulate the pulse shaping through changing phase difference $\Delta\varphi$. Figure 11 is the simulation result when $\Delta\varphi$ is changed from 0 to π, and other variables are set as: $A_1 = A_2 = 1$, $\theta = 10°$, and $\Delta T = 5$ ps. In Figs. 11(a)–11(e), we can see that horizontal polarization mode is always bright soliton with multiple side peaks, while vertical polarization mode is always black soliton with chirp-like oscillated pulses at pulse trailing edge position. Figures 11(f)–11(j) are the

corresponding optical spectra, which show that the horizontal mode has higher/lower peak intensity at 1063 nm/1067 nm compared with the vertical mode, and the wavelength splits at 1067-nm position for both orthogonal polarization modes.

It should be noted that the simulation results in Figs. 9, 10, and 11 are different. For pulse shapes in Fig. 9, the vertical dark soliton has side pulse oscillations at pulse leading edge when ΔT is not larger than 3 ps, while in Figs. 11(a)–11(e), the vertical dark soliton always has smooth pulse leading edge with different $\Delta\varphi$ values. For optical spectra in Fig. 10, both orthogonal modes have multiple side peaks at 1067 nm and the number of peaks decreases with increased ΔT. While in Figs. 11(f)–11(j), the number of side peaks at 1067-nm position is almost unchanged.

3. Conclusion

We simulated the pulse shaping of bright–dark vector soliton pair at 1-μm wavelength region. Through changing input pulse pair parameters, various kinds of pulse shapes and optical spectra can be generated. When the orthogonal modes have the same central wavelength, "2+2"- and "1+2"-type pseudo-high-order polarization-locked bright–dark vector soliton pairs can be generated. While for different central wavelengths, group-velocity-locked bright–dark vector soliton pairs with chirp-like oscillated pulses at pulse trailing edge position can be generated. Our simulations can provide beneficial conduct for experiments about pulse shaping of bright–dark vector soliton pair with different wavelengths.

References

[1] Song Y F, Shi X J, Wu C F, Tang D Y and Zhang H 2019 *Appl. Phys. Rev.* **6** 021313
[2] Luo Z C, Liu M, Luo A P and Xu W C 2018 *Chin. Phys. B* **27** 094215
[3] Zhou Y, Zhang R L, Li X, Kuan P W, He D Y, Hou J S, Liu Y F, Fang Y Z and Liao M S 2019 *Chin. Phys. B* **28** 094203
[4] Chen S, Xu Y, Cai Y, Shen J P and Zhang Z X 2019 *J. Opt. Soc. Am. B* **36** 2688
[5] Yin K, Li Y M, Wang Y B, Zheng X and Jiang T 2019 *Chin. Phys. B* **28** 124203
[6] Wang Z Q, Zhan L, Fang X and Luo H 2017 *J. Opt. Soc. Am. B* **34** 2325
[7] Chong A, Wright L G and Wise F W 2015 *Rep. Prog. Phys.* **78** 113901
[8] Duan L N, Wen J, Fan W and Wang W 2017 *Chin. Phys. B* **26** 104205
[9] Zhou Y, Zhang R L, Chen P, Liu Y F, Fang Y Z, Wang T X, Li X, Kuan P W and Liao M S 2019 *Laser Phys.* **29** 055101
[10] Luo Z C, Lin Z B, Li J Y, Zhu P F, Ning Q Y, Xing X B, Luo A P and Xu W C 2014 *Chin. Phys. B* **23** 064203
[11] Zheng Y, Tian J R, Dong Z K, Xu R Q, Li K X and Song Y R 2017 *Chin. Phys. B* **26** 074212
[12] Wang H C, Wei Y D, Huang X Y, Chen G H and Ye H 2018 *Chin. Phys. B* **27** 044203
[13] Zhao J Q, Zhou J, Li L, Zhao L M, Tang D Y, Shen D Y and Su L 2019 *Opt. Lett.* **44** 2414
[14] Xiong Z J, Xu Q and Ling L M 2019 *Chin. Phys. B* **28** 120201
[15] Liu B W, Luo Y Y, Xiang Y, Xiao X P, Sun Q Z, Liu D M and Shum P P 2018 *Opt. Express* **26** 27461
[16] Liu X M, Yao X K and Cui Y D 2018 *Phys. Rev. Lett.* **121** 023905
[17] Liu X M and Pang M 2019 *Laser Photon. Rev.* **13** 1800333
[18] Liu X M and Cui Y D 2019 *Adv. Photon.* **1** 016003
[19] Liu X M, Popa D and Akhmediev N 2019 *Phys. Rev. Lett.* **123** 093901
[20] Balla P and Agrawal G P 2018 *J. Opt. Soc. Am. B* **35** 2302
[21] Cundiff S T, Collings B C, Akhmediev N N, Soto-Crespo J M, Bergman K and Knox W H 1999 *Phys. Rev. Lett.* **82** 3988
[22] Collings B C, Cundiff S T, Akhmediev N N, Soto-Crespo J M, Bergman K, Knox W H 2000 *J. Opt. Soc. Am. B* **17** 354
[23] Tang D Y, Zhang H, Zhao L M and Wu X 2008 *Phys. Rev. Lett.* **101** 153904
[24] Jin X X, Wu Z C, Li L, Zhang Q, Tang D Y, Shen D Y, Fu S N, Liu D M and Zhao L M 2016 *IEEE Photon. J.* **8** 1501206
[25] Wang X, Li L, Geng Y, Wang H X, Su L and Zhao L M 2018 *Appl. Opt.* **57** 746
[26] Xiang Y, Luo Y Y, Liu B W, Xia R, Shum P P, Tang X H, Liu D M and Sun Q Z 2019 *J. Lightwave Technol.* **37** 5108
[27] Zhu S N, Wu Z C, Fu S N and Zhao L M 2018 *Appl. Opt.* **57** 2064
[28] Zhao L M, Tang D Y and Wu X 2008 *Opt. Express* **16** 10053
[29] Liu M, Luo A P, Luo Z C and Xu W C 2017 *Opt. Lett.* **42** 330
[30] Willner A E, Wang J and Huang H 2012 *Science* **337** 655
[31] Su Y L, Feng H, Hu H, Wang W, Duan T, Wang Y S, Si J H, Xie X P, Yang H N and Huang X N 2019 *Chin. Phys. B* **28** 024216
[32] Ma J, Shao G D, Song Y F, Zhao L M, Xiang Y J, Shen D Y, Richardson M and Tang D Y 2019 *Opt. Lett.* **44** 2185
[33] Hu X, Guo J, Shao G D, Song Y F, Yoo S W, Malomed B A and Tang D Y 2019 *Opt. Express* **27** 18311
[34] Zhou Y, Li Y F, Zhang R L, Wang T X, Bi W J, Li X, Kuan P W, Fang Y Z and Liao M S 2019 *Optik* **194** 163132
[35] Zhou Y, Li Y F, Li X, Zhao G Y, Hou J S, Zou J, Fang Y Z and Liao M S 2020 *Optik* **203** 163925